High Temperature Superconducting Resonators and Switches: Design, Fabrication, and Characterization

Milton Feng, *Fellow, IEEE,* Frank Gao, *Member, IEEE,* Zhongmin Zhou, Jay Kruse, *Member, IEEE,* Matt Heins, Jianshi Wang, S. Remillard, R. Lithgow, M. Scharen, A. Cardona, and R. Forse

Abstract— **We report our recent efforts in designs of several RF and microwave devices using high temperature superconducting (HTS) thin film technology. Devices considered include transmission lines, resonators, switches, and phase shifters in microstrip, stripline and coplanar waveguide. The circuit design, modeling, simulation, fabrication, packaging, and testing are discussed. Using a two-dimensional (2-D) EM simulator, we have optimized the geometry of the RF microstrip and stripline resonators for frequencies near 900 MHz. An unloaded Q is obtained as high as 80,000, three orders of magnitude greater than the traditional 2-D gold or copper resonators with identical structures. On-wafer probe and bit-error rate measurements show that the HTS transmission lines have an extremely small insertion loss and dispersion; thus they are ideal candidates for applications in multichip module interconnects and delay lines. A sharp switching characteristic and an unusually strong RF power hysteresis loop have been observed in the HTS lines. This interesting behavior has been utilized for designs of new HTS microwave phase shifters. The use of HTS lines can substantially reduce the losses suffered by conventional PIN diode switches.**

I. Introduction

APPLICATIONS of high-temperature superconductors (HTS) on passive and active microwave circuits are of interest because of the extremely low loss and dispersion. HTS microwave components being used or that are under development include transmission lines, multichip module interconnects, delay lines, Josephson Junction antennas, resonators, and filters [1], [2]. Strong interest also lies in hybrid and monolithic microwave integrated circuits (MMIC) that integrate GaAs active devices [3]. To explore such potential applications, it is essential to accurately characterize the devices at low temperatures and high microwave power [4]–[6]. Such investigations can be used to devise accurate models for use in microwave design.

We are developing a variety of HTS microwave passive and active devices on coplanar transmission lines, high-Q resonators, superconducting switches, and low loss phase shifters. This work outlines our activities in HTS thin film characterization, passive and active device design, modeling, simulation, fabrication, and testing. The scattering parameter and bit-error rate measurements on patterned $YBa_2Cu_3O_7$ (YBCO) transmission lines demonstrate extremely small insertion loss and dispersion. An interesting switching behavior has been found from RF power measurements in the wireless communication band. This behavior is exploited in the novel design of an HTS phase shifter.

II. High Frequency Surface Resistance

Microwave surface resistance R_s is one of the most important parameters in identifying high quality materials for device fabrication. We have developed an experimental system for thin film R_s measurement using a parallel-plate resonator (PPR) technique as first introduced by Taber [7]. A schematic of our setup is illustrated in Fig. 1. The PPR was constructed using two identical unpatterned (1 cm × 1 cm) superconducting thin films grown on low loss dielectric wafers (typically MgO or $LaAlO_3$). A 12.5-μm thick teflon dielectric spacer ($\varepsilon = 2.04$) was sandwiched between the superconducting samples to form the resonator structure. The resonator was then positioned at the center of a copper cavity to shield the radiation loss. Two semirigid coaxial cables were used to excite a resonant mode in the cavity. A thermal sensor and an electric heater were mounted on the copper cavity, and the setup was placed in a liquid helium dewar for cryogenic measurements. The resonant frequency and Q factor were determined by a curve fitting to the S-parameters [8] measured with a Hewlett Packard 8510 vector network analyzer. This system allowed us to determine experimentally the complex surface impedance, penetration depth, complex conductivity, and quasi-particle scattering time [9].

Manuscript received October 15, 1995; revised February 15, 1996. This work was supported by the National Science Foundation under DMR-91-20000 through the Science and Technology Center for Superconductivity.

M. Feng and M. Heins are with the Science and Technology Center for Superconductivity, Microelectronics Laboratory, Department of Electrical and Computer Engineering, University of Illinois at Urbana-Champaign, Urbana, IL 61801 USA.

F. Gao was with the Science and Technology Center for Superconductivity, Microelectronics Laboratory, Department of Electrical and Computer Engineering, University of Illinois at Urbana-Champaign, Urbana, IL 61801 USA. He is now with M/A-COM Inc., Integrated Circuits Business Unit, Lowell, MA 01851 USA.

Z. Zhou was with the Science and Technology Center for Superconductivity, Microelectronics Laboratory, Department of Electrical and Computer Engineering, University of Illinois at Urbana-Champaign, Urbana, IL 61801 USA. He is now with Viewsonics, Inc., Boca Raton, FL USA

J. Kruse was with the Science and Technology Center for Superconductivity, Microelectronics Laboratory, Department of Electrical and Computer Engineering, University of Illinois at Urbana-Champaign, Urbana, IL 61801 USA. He is now with Watkins-Johnson, Palo Alto, CA USA.

J. Wang was with the Science and Technology Center for Superconductivity, Microelectronics Laboratory, Department of Electrical and Computer Engineering, University of Illinois at Urbana-Champaign, Urbana, IL 61801 USA. He is now with Advanced Micro Devices, Sunnyvale, CA USA.

S. Remillard and R. Lithgow are with the Illinois Superconductor Corporation, 451 Kingston Court, Mt. Prospect, IL 60056 USA.

M. Scharen, A. Cardona, and R. Forse are with Superconductor Technologies Incorporated, Santa Barbara, CA 93111-2310 USA.

Publisher Item Identifier S 0018-9480(96)04805-3.

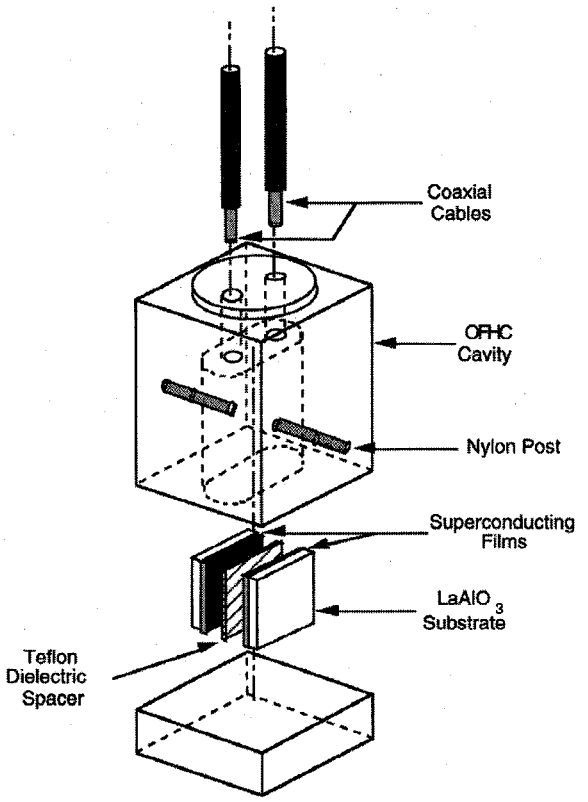

Fig. 1. Schematic of the parallel plate resonator (PPR) setup used for microwave surface impedance measurements on superconducting thin films. This system has a high sensitivity to resonant frequency shift and high surface resistance resolution (10 $\mu\Omega$).

Fig. 2 shows the typical surface impedance of the YBCO films (T_c = 90 K) used for device fabrications. The 10-GHz loss is 450 $\mu\Omega$ at 77 K and ~150 $\mu\Omega$ at $T \ll T_c$. Unlike ordinary metals, the HTS surface reactance $X_s \gg R_s$, indicating that a superconductor is an inductive element in microwave circuit.

III. Cryogenic Microwave On-Wafer Probe Techniques

In evaluating the performance of a planar circuit, extrinsic factors introduced by parasitics [10] are excluded by taking on-wafer probe measurements before the device is packaged. In addition, an accurate network analyzer calibration is critical to remove systematic errors caused by test port mismatch, leakage, and frequency response. A line-reflect-match (LRM) technique was used in the calibration of the network analyzer. Calibration was performed at each temperature of interest to account for temperature dependence in the electrical behavior of probe elements and feed throughs.

Fig. 3 illustrates the cryogenic probe system for on-wafer S-parameter measurements. The probes are aligned in a ground-signal-ground configuration. Liquid helium or nitrogen can be used as cryogen to vary the sample temperature between 20–300 K. The chamber was evacuated below 1 mTorr using a turbo-molecular pump. A radiation shield was added to isolate the cold station from thermal radiation of the chamber body, and copper-tin braids were attached from the bottom of the

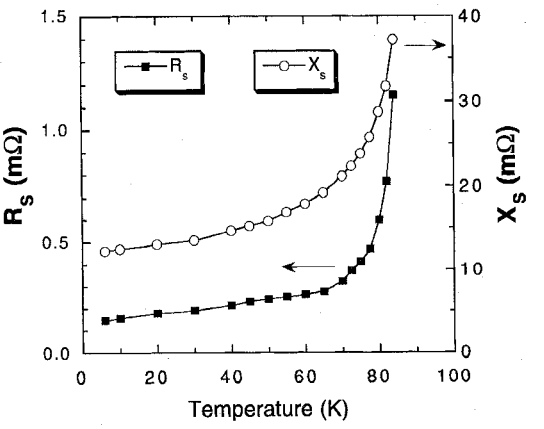

Fig. 2. The resistive (R_s) and inductive (X_s) parts of the surface impedance measured with the PPR technique at 10 GHz for two YBCO thin films. These films were grown epitaxially on 0.5-mm-thick $LaAlO_3$ by *in situ* off-axis sputtering at Conductus. The R_s is two order of magnitude smaller than X_s (inductive response dominant) and is about 50 times smaller than the surface resistance of copper.

cold stage to the top of the microwave probe to minimize the thermal gradient when probes contacted the device under test (DUT).

IV. Attenuation, Dispersion, and Bit Error Rate of HTS Lines

Fig. 4 shows the coplanar meander structure of the ion-milled, gold and YBCO lines which were patterned on 0.5-mm-thick MgO ($\varepsilon = 9.8$) wafers. The lines had a length of 6 cm, width of 8 μm, and a strip to ground spacing of 4 μm. Because of the direct coupling to the line, the magnitudes of the RF fields (H_{rf}) and the current density (J_{rf}) can be easily estimated at a given input power. The calculated characteristic impedance of our CPW transmission lines was 51 Ω [11]. Contact pads were added such that the scattering parameters of the lines could be measured with 150 μm pitch microwave probes [12]. The sample was mounted over the on-wafer probe cold station shown in Fig. 3.

The two-port S-parameter data from CPW line measurements can provide convincing evidence that HTS lines have considerably smaller insertion loss than similar gold lines. Fig. 5 demonstrates such comparison for a frequency range of 0.1–10 GHz. The attenuation constant at 3 GHz was 0.28 Np/m for the HTS line and 14 Np/m for the gold line. Both of these gold and YBCO lines were fabricated with a standard photolithography process at the Superconductor Technologies Incorporated (STI). The gold line was 0.7-μm thick and the laser ablated YBCO was 0.9-μm thick.

After on-wafer testing, both samples were packaged by gold plated stainless steel fixtures and wire-bonded to microwave connectors via two 5-mm-long gold microstrip lines. These packaged lines were connected to the Hewlett Packard Bit Error Rate (BER) tester and Tektronix 11 801A Digital Scope by two flexible 30-cm coaxial cables. The tester consists of an HP70841 pattern generator (0.1–3 Gbit/s), an HP70311 clock source (0.016–3.3 GHz), and an HP 70842 error detector (0.1–3 Gbit/s). Eye-diagram and BER measurements present an innovative approach to characterizing the transmission

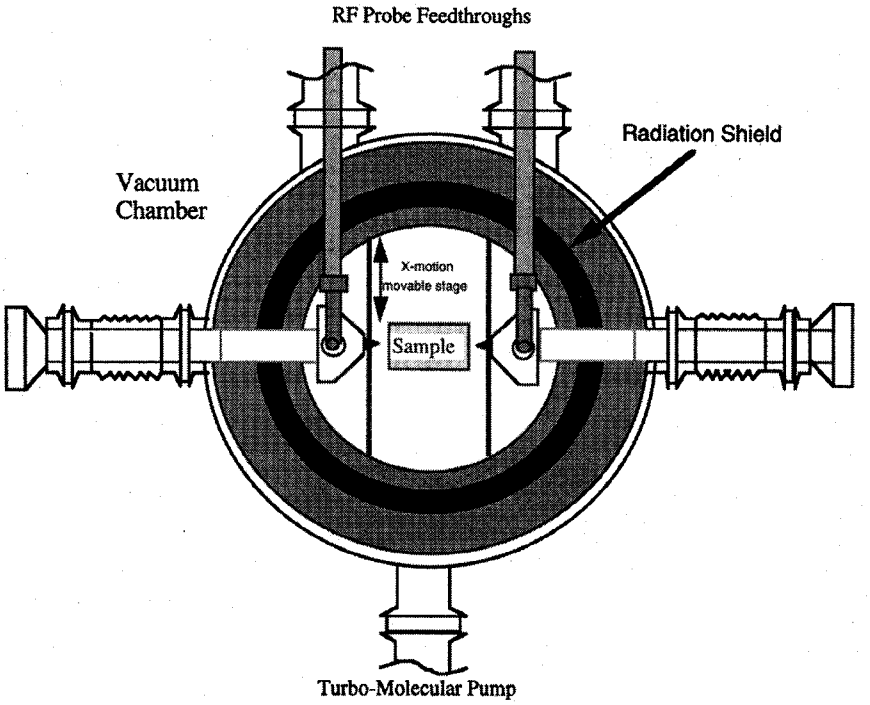

Fig. 3. Cryogenic on-wafer-probe experimental system for microwave scattering parameter and insertion loss measurements.

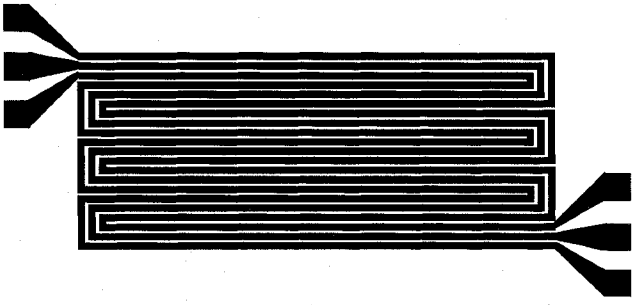

Fig. 4. Schematic layout of the 6-cm-long coplanar transmission line on a 0.5-mm-thick MgO substrate. Center conductor width is 8 μm and the spacing between center line and ground is 4 μm, giving a characteristic impedance of 51 Ω. The pad pitch is 150 μm for use with microwave probe measurement.

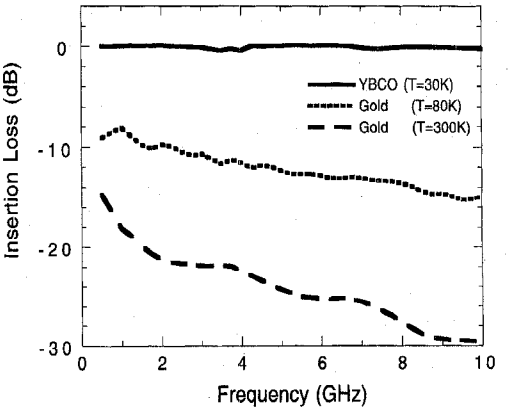

Fig. 5. Insertion loss obtained by on-wafer measurements for 6-cm-long YBCO and gold coplanar transmission lines. The insertion loss of the HTS line was -0.12 dB at a frequency of 3 GHz compared to -10.7 dB for the gold line at 80 K.

lines. The validity of using HTS lines in multichip modules can be assessed by varying the data rate and the pseudo random bit sequence (PRBS). Eye diagram analysis using an HP71604B bit error rate tester indicates a superior performance of the YBCO coplanar line, as demonstrated in Fig. 6. For comparison, a 30-cm flexible coaxial transmission line has been used as a standard reference. In addition to its low attenuation and dispersion, the rise time (150 ps) of the HTS line is faster than that of the gold line (180 ps) and is very near the limit of the measurement setup. The pulse width and height for the HTS line were 270 ps and 350 mV compared to 225 ps and 100 mV for the gold line. In other words, the "eye area" of the gold line is much less than the HTS line. Such eye area is a visual indication of the probability of error. When the eye becomes closed, the probability of transmitting errant data bits increases.

The bit error rate data illustrate severe penalties of using conventional lossy lines at microwave frequencies. The packaged gold line at room temperature would be unable to transmit data accurately above 2 Gbit/s since the BER increases substantially at clock rates above 2 Gbit/s (Fig. 6). The HTS line at 77 K has a bit error rate of less than 10^{-11} at 3 Gbit/s.

V. High Power Transmission and Switching Effect of HTS Lines

Power measurements over the wireless communication band (0.8–2 GHz) were carried out using an HP8350 synthesized sweeper. The microwave signal was boosted by a PST-AR8829 solid-state power amplifier to a maximum of 10 W (see Fig. 7). A step attenuator was used to vary the incident power at the device under test (DUT), and a low pass filter was

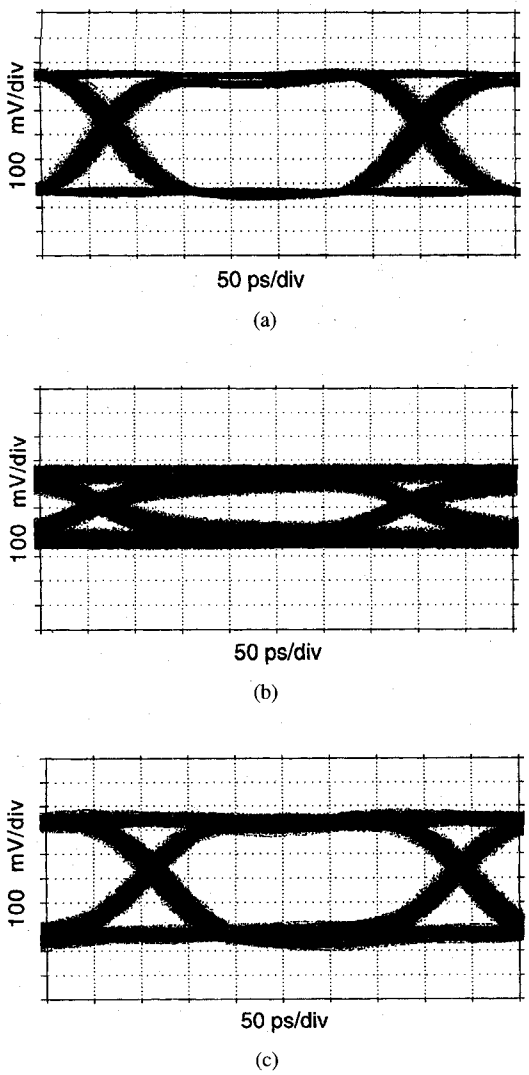

Fig. 6. Eye-diagram of a standard flexible coaxial transmission line (30 cm) at room temperature used as a reference (a), and packaged 6-cm gold (b) and YBCO (c) coplanar transmission lines at 77 K. The clock frequency is 3 Gbit/s with a word length of $2^{10}-1$. The gating period was 100 s and the threshold level was 10^{-3}. The YBCO line exhibits very little attenuation and dispersion compared to the gold line.

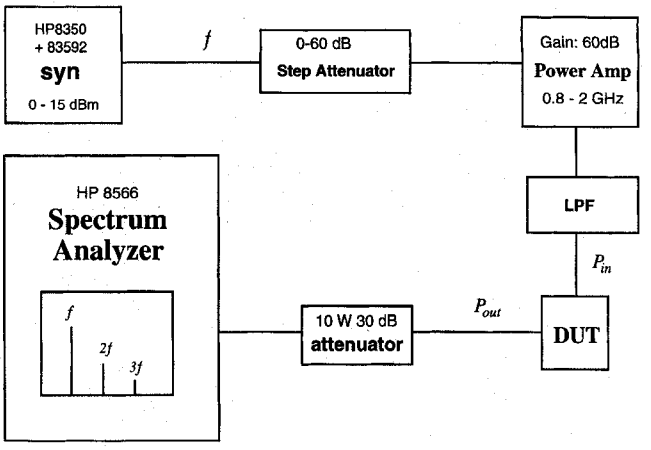

Fig. 7. Schematic block diagram of the high RF power measurement system used for testing two-port devices (transmission line, resonator, filter, or amplifier) over a frequency range of 0.8–2 GHz.

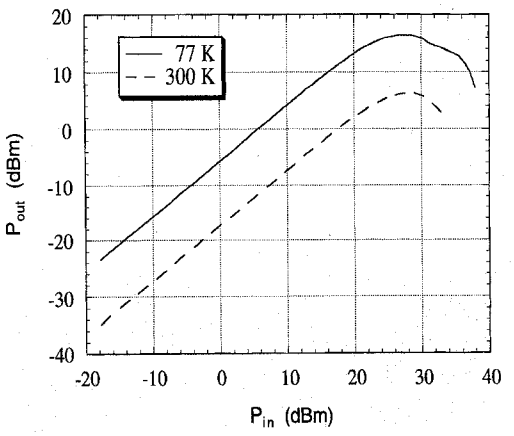

Fig. 8. Compression curve for a 6-cm coplanar gold transmission line at a frequency of 1 GHz and at temperatures of 77 and 300 K.

inserted between the power amplifier and the DUT to eliminate harmonics generated by the equipment system. The power signal was injected into one end of the DUT (the packaged transmission line), and the transmitted signal was monitored using an HP8566 spectrum analyzer. Calibration was carefully performed to obtain the power at the input and output of the DUT. A 30-dB attenuator was used to prevent the RF power from overdriving the spectrum analyzer. At high power level, harmonics from the nonlinearity of the DUT can be detected by the spectrum analyzer. The devices used for high power measurements were packaged gold and YBCO lines. They were the same samples as that used for other experiments shown in Figs. 5 and 6.

Fig. 8 plots the transmitted power versus the input power at 1 GHz for the gold line at both liquid nitrogen and room temperatures. At low power levels, it exhibits a linear increase (slope = 1), as expected. The insertion loss is 6 dB at 77 K and 17 dB at 300 K, due to increasing resistivity with temperature. As the RF power increases, the curves tend to saturate. However, there is no appreciable change of the 1-dB-compression point (21 dBm) or the saturation point (28 dBm) as T is brought from 77 to 300 K. A rapid drop is seen in P_{out} for P_{in} >30 dBm (1 W).

We now focus on the results of the HTS YBCO line (Fig. 9). There are several characteristics that are distinct from those of the gold line. First, in the linear regime (a–b), the HTS sample suffers only 0.2 dB insertion loss. Second, the curve (b–c) shows an abrupt drop by 37 dB in P_{out} when the driving power reaches a critical level of $P_c = 26$ dBm = 398 mW at point b. Third, with P_{in} further increased (c–d), the transmitted power P_{out} increases again with a slope of only 0.62, deviating significantly from a linear increase. Unlike the gold line, no saturation is observed up to $P_{in} = 31.5$ dBm (1.52 W). Fourth, as P_{in} is then reduced (e–f), P_{out} retraces the previous curve only until $P_{in} = P_c$. Finally, and most interestingly, as P_{in} is reduced further P_{out} does not jump back to point b but follows a new path down to point g where $P_{in} = 0.4P_c = 22$ dBm (158 mW), after which P_{out} starts to grow rapidly by ~28 dB and finally returns to the linear regime for $P_{in} < 0.18P_c = 18.5$ dBm (71 mW) as shown in curve g–h–i. The curve is thus hysteretic. All features described

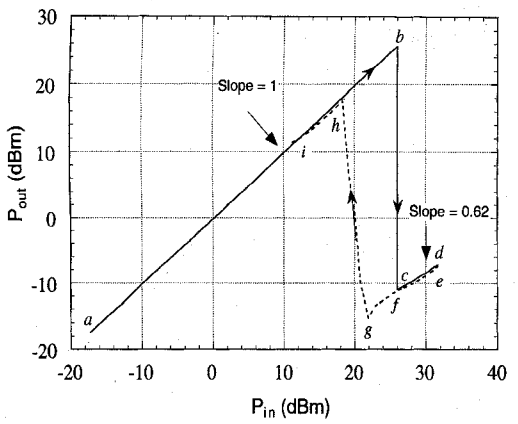

Fig. 9. Microwave power dependence for a 6-cm coplanar $YBa_2Cu_3O_7$ transmission line on MgO wafer at 1 GHz and 77 K, showing a pronounced hysteresis loop. In the linear regime (a–b), it has a negligible insertion loss which is much smaller than that in the gold line shown in Fig. 8. The solid curve (a–b–c–d) describes a process with *increasing* incident power (P_{in}) and the dashed curve (e–f–g–h–i) illustrates the process with *decreasing* P_{in}. Data are collected with P_{in} varied in 0.5 dBm steps.

above are highly reproducible in repeated experiments. Such a sharp drop in P_{out} and strong hysteretic power dependence are unique to the pattered high-T_c superconducting line. The gold line with an identical planar structure does not exhibit any of these characteristics (see Fig. 8).

The transmission line would remain in a superconducting Meissner state at low RF driving power as long as the magnetic field, H_{rf}, is smaller than the lower critical field of the superconductor. Because the Cooper pairs that carry the supercurrent do not suffer from scattering, the HTS line has a negligible insertion loss and all incident power is delivered to the output load. Thus $P_{out} = P_{in}$ as represented by the linear regime (a–b). At point b, a peak RF current of 126 mA is generated along the center strip and the surface RF field is $H_{rf} = 97$ Oe, on the same order of the dc lower critical field, H_{c1}. It is reasonable to introduce a critical RF field, $H_{c1}^{\rm rf}$, above which vortex creation and flux penetration become possible and the surface resistance increases rapidly [4]. Due to the screening effect, the current is primarily constrained within a layer equal to the penetration depth $\lambda(T)$, which is $\sim 0.3\,\mu$m at 77 K for YBCO. The average RF current density at point b would be $J_{rf} = 2.6 \times 10^6$ A/cm^2, assuming uniform current distribution over the width and the $\lambda(T)$ of the line. In reality the current density is much larger near the edges and is smaller near the center than this average value due to a current crowding effect [13]. The J_{rf} value estimated above is comparable to the dc critical current (J_c) of YBCO reported in literature. The sharp "switch-off" at point b has been attributed [14] to overdriving the HTS line above its RF critical current $J_c^{\rm rf}$, switching the material to a "normal state."

Once the line becomes nonsuperconducting, the incident power is dissipated almost entirely on the transmission line due to a much larger R_s. The thermal quenching by power absorption maintains the film above T_c. The curve shows a history dependence and, as P_{in} is reduced, it goes through e–f–g–h–i instead of e–f–b–i. Therefore, the material must experience a different process when P_{in} is reversed. Unlike the process along a–b, in which the current is carried by Cooper pairs and the sample essentially remains 77 K as P_{in} is increasing, the sample temperature in process f–g may be above T_c. Although it could have $J_{rf} \ll j_c^{\rm rf}$ because the current is carried by the normal electrons, the large amount of incident power dissipated on the lossy line has to be reduced further until the liquid nitrogen can carry away the heat and cool off the sample across T_c to return to a superconducting state. In summary, the sharp b–c drop is a phase transition triggered by exceeding the threshold of $J_c^{\rm rf}$, whereas the broad g–h transition is primarily a thermal cooling process by reducing the RF power absorption [14].

The features found in this work can be utilized in designs of HTS microwave power and current limiters. When the flowing RF current exceeds a designated critical value, the HTS line undergoes an abrupt transition and the current to a load will be cut off or greatly reduced. The minimum I_{rf} needed to switch the circuit off can be controlled by varying the linewidth, and the switching speed can be enhanced using a shorter line or by overstepping the critical current. The circuit can return normal operation by reducing the driving power to point h. We will outline our approaches in using this behavior for applications of switches as replacement of conventional semiconductor P_{in} diode switches that have larger forward-bias insertion loss.

VI. High-Q HTS RF Resonator Design, Simulation, and Fabrication

Resonate elements are still of great interest, especially for microstrip and stripline filters. High Q and compact resonators are essential in wireless communication applications which require very low loss and very narrow bandpass filters. HTS resonators are attractive because of the extremely small attenuation and dispersion of the HTS lines as discussed above. We report our efforts in design of planar $\lambda/2$ HTS resonators that potentially have an unloaded Q above 80 000 at $\sim$1 GHz when operating at liquid nitrogen temperature.

Computer aided design (CAD) software packages play an important role in microwave circuit analysis and optimization. The HP Momentum simulator,together with the HP Microwave Design System (MDS), have been used to carry out the modeling and simulations for resonators in microstrip, stripline, and coplanar waveguide structures. Momentum uses a numerical procedure, based on the method of moments, to solve the circuits in 2-D planar geometry. The structures are divided into *meshes* (grid-like pattern of rectangles and triangles) described by a mesh frequency f_{mesh}, and the planar solver calculates the circuit response. The results are typically S-parameters and the strength of the elctro-magnetic fields propagating through the circuit layout can be visualized.

Fig. 10 illustrates the open-end *linear* and *U-shape* $\lambda/2$ resonators studied using the HP Momentum simulator. To optimize resonator performance, we examined each of the circuits by varying a set of the geometry parameters such as the linewidth, curvature, coupling gap, and feedline length. Fluctuation arising from other material-dependent parameters such as conductor surface impedance, substrate dielectric constant and loss tangent was also carefully investigated. The

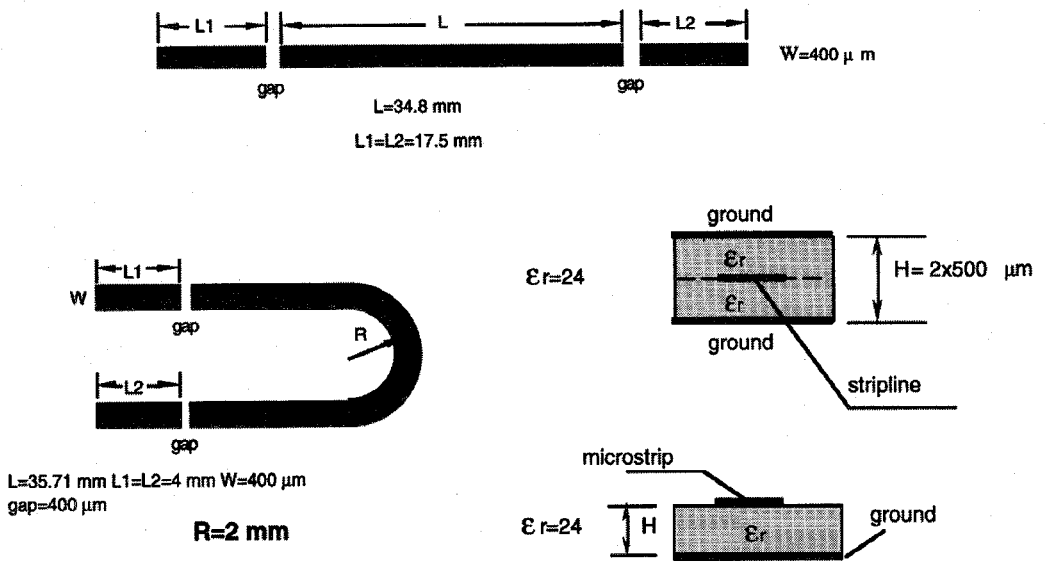

Fig. 10. Design layout of superconducting high-Q microstrip and stripline RF resonators.

TABLE I
SIMULATION RESULTS OF THE OPTIMIZED DESIGNS OF SUPERCONDUCTING STRIPLINE RESONATORS (SEE FIG. 10) OPERATING AT 850 MHz AND 77 K

850MHz STRPR: L = 35.71mm; W = 400μm; Gap = 400μm; H=2 × 500 μm Zs=(0.00338+j2.19) mΩ; GND=HTS; tanδ=7.6×10^{-6} f_{mesh} = 2 GHz			
Layout	f_0(MHz)	$Q_L(10^3)$	$Q_u(10^3)$
Straight line	850.05	43.8	81.4
U-shape(0° feedlines) R=2 mm	850.94	43.4	81.7
U-shape(90° feedlines) R=2mm	851.80	24.5	82.1

resonators designed were under coupled, and the intrinsic or unloaded Q was extracted by either increasing the coupling gaps or using the following equations [15]:

$$\beta_1 = \frac{1 - S_{11}}{S_{11} + S_{22}},$$
$$\beta_2 = \frac{1 - S_{22}}{S_{11} + S_{22}},$$
$$Q_u = Q_L(1 + \beta_1 + \beta_2)$$

where β_1 and β_2 are the coupling coefficients at port 1 and port 2, respectively. S_{11}, S_{22} are the magnitudes of the S-parameters measured at the resonant frequency. Despite a strong dependence of the loaded Q on the feedline or coupling gap length, the Q_u obtained using the above equations essentially remained constant. The loaded Q rapidly converged and approached Q_u as the gaps were widened. After optimizing the layout geometry, the Q_u of a $\lambda/2$ stripline resonator (with the center strip and ground planes being $YBa_2Cu_3O_7$ films) at $T = 77$ K near 1 GHz was found to be ~80 000. Identification of the intrinsic Q is essential for an eventual consideration of band-pass filter design.

Table I tabulates the simulation results for the YBCO/$LaAlO_3$ stripline resonators operating at 850 MHz. Here we have scaled the Z_s values in Fig. 2 to 850 MHz assuming $R_s \propto \omega^2$ and $X_s \propto \omega$. A typical loss tangent value for $LaAlO_3$ [16] was used. Similar simulation results were also obtained for microstrip and CPW structures, with the resonant frequency increased to about 1.2 GHz due to a decreased effective dielectric constant. For convenience of performing ground-signal-ground on-wafer probe measurements, we have also configured a U-shaped resonator with the feedlines perpendicular to the strip (90° feedlines). The simulated results clearly show that the HTS resonators exhibit considerably superior performance to normal metal resonators at RF and microwave frequencies. Our simulations of Au resonators with identical structures at 77 K and 875 MHz only resulted in a $Q_u \sim 200$, almost three orders of magnitude lower than that of HTS resonators. At room temperature, the Q for the gold resonator dropped to 28. We also found that HTS materials must be used for the ground planes in order to keep such superior performance. A dramatic decrease in Q would occur if metallic ground planes were used instead.

After optimizing the circuit geometry with the 2-D simulator, the lift-off (negative) and ion milling (positive) processes were performed in device patterning. The YBCO and gold resonators were patterned onto 0.5-mm thick, two-inch diameter $LaAlO_3$ wafers. For lift-off processing, the samples were fabricated with photolithography to form the CPW resonator structures. Briefly, the 2-inch $LaAlO_3$ wafer was cleaned with hot TAM (Trichloroethylene, Acetone, Methanol) solutions (2 min each), rinsed with Isopropanol, and dried with nitrogen gas. The wafer was then coated with Photoresist (PR) 1813 and spun for 30 s at 5000 rpm to give a uniform film of about 1 μm thick. After soft baking for 60 s at 120°C to improve resist adhesion, the wafer was aligned to the "negative" mask and the PR was exposed to ultraviolet light illumination of 11 mW/cm^2 for 18 s. The pattern was developed in solution 352 for 60 s to remove the exposed PR areas. A 1-μm thick gold film was evaporated onto the substrate and the PR. The final pattern transfer was completed with a lift-off process. The portions of the Au film on the resist were removed by dissolving the PR layer in liquid etchant so that the overlying gold film was lifted. Similarly, for ion milling processing, the HTS or gold film was first evaporated onto a cleaned wafer. PR was then coated, spun, baked, and afterward was covered with a "positive" mask for exposure to light and developing. The final pattern was obtained by removing the exposed part of the film using an ion-milling (dry etching) process.

Fig. 11 plots the measured S-parameters for an ion-milled, U-shaped (90° feedlines) gold CPW resonator from 1–2 GHz, at room temperature. The resonant frequency is 1.17 GHz. For $LaAlO_3$, $\varepsilon = 24$. An approximate effective dielectric constant for this CPW structure is $\varepsilon_{eff} = (\varepsilon + 1)/2 = 12.5$. The estimated resonant frequency is $f = c/(2L\sqrt{\varepsilon_{eff}}) = 15/(3.571\sqrt{12.5}) = 1.188$ GHz, in excellent agreement with the measured value. (In a stripline structure, the resonant frequency would be ~850 MHz.) The upturn in S_{21} at high frequency is due to a second harmonic centered near 2.4 GHz. The loaded Q is only 14. Since conductor loss is dominant, one expects that the loaded Q at liquid nitrogen temperature would be about five times larger. The HTS resonators are being processed for future testing. The Q should be greatly enhanced since the conductor loss is much smaller than Au at RF frequencies.

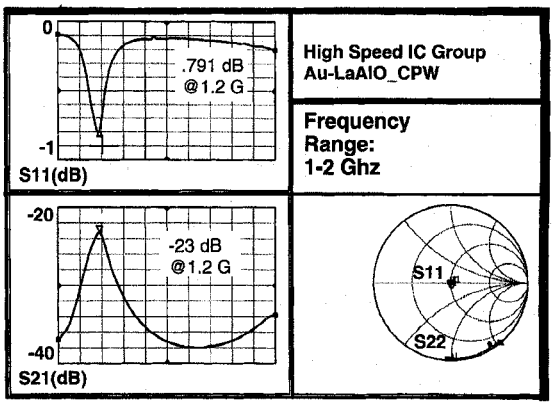

Fig. 11. Measurement data for an ion-milled gold coplanar waveguide resonator on $LaAlO_3$ substrate at 300 K.

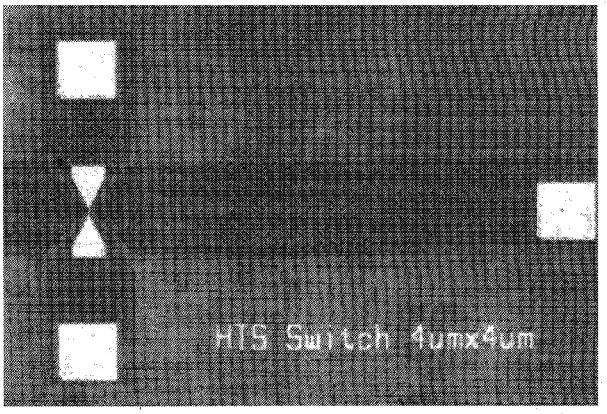

(a)

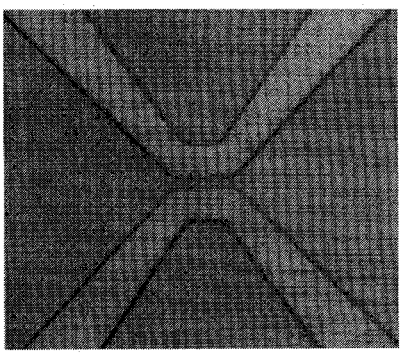

(b)

Fig. 12. The pictures of an HTS switch for the microbridge (a) and a 1 μm-wide HTS coplanar line and (b) generated by ion milling process.

VII. HTS Switch

We have fabricated an HTS switch, which is shown in Fig. 12(a). This kind of HTS switch is actually a cross structure, in which the HTS transmission line narrows down to about 2 μm as shown in Fig. 12(b). A thin, narrow gold film lies on the top of HTS microbridge vertically with a thin insulation layer in between. DC power will be added to the gold film to increase the temperature locally on the cross in order to reduce the local critical current of the HTS or even drive the cross to a nonsuperconducting state, if desired. According to the power characteristics in the measurement of Fig. 9, cutoff of a microwave signal will be expected along the HTS line. The threshold power for the cutoff strongly depends on the dimension of the cross. For the measurement of Fig. 9, the data was obtained for a long transmission line (6 cm long and 8 μm wide). However, for the HTS switch, the microbridge length is just about 10 μm. So we can expect to spend very small power to control the microwave signal going through the line and shorten the switching time significantly. Presently, these devices are being tested.

VIII. HTS Phase Shifter

Conventional microwave phase shifters have limited use due to large insertion loss from metal conductors and semiconductor P_{in} diode switches. Recently, hybrid digital phase shifters have been developed by replacing the metal conductors with

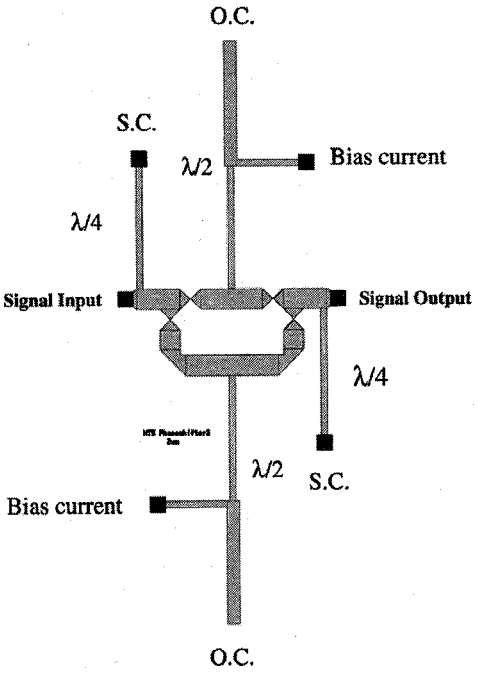

Fig. 13. Layout design of a microstrip HTS phase shifter fabricated with YBCO on $LaAlO_3$. Bias current indicates the dc bias inputs. S.C. denotes a short-circuit to ground for the dc current return, and O.C. denotes an open-circuit. The black squares represent the gold pads for ohmic contact. The overall dimensions of the structure is ~2 mm × 4 mm.

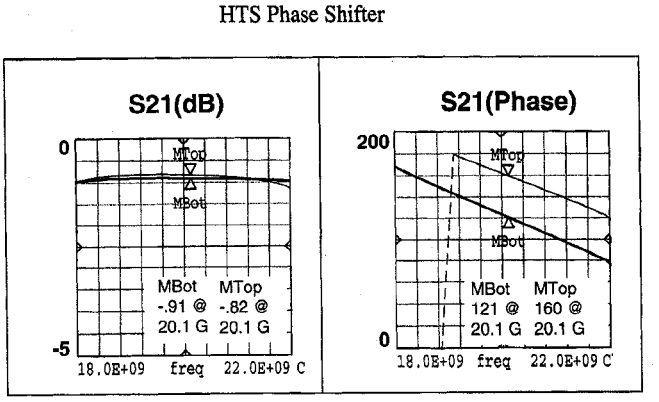

Fig. 14. Simulation results of the high-T_c superconducting phase shifter in a structure as shown in Fig. 13. The insertion loss is less than 1 dB and the phase shift is 45° at 20 GHz.

HTS materials, reducing the conductor loss by 1.5–2 dB [17]. However, the P_{in} diodes used still contribute significant losses (typically 1.5 dB per diode) to the circuit. In this work, we report our design of new phase shifters using all HTS material for phase delay and switching based on the features illustrated in Fig. 9. This is an attractive technology because the HTS phase shifter can be realized in a monolithic geometry, and can eliminate the large insertion losses contributed by both the metal conductors and P_{in} diode switches.

The physical layout of one type of phase shifter is depicted in Fig. 13. The entire phase shifter is a microstrip transmission line made of YBCO film. The width of the main signal line is 160 μm. Points where the triangles meet are locations of the micro-bridges with dimensions of 2 μm × 10 μm. These microbridges provide the switches needed to direct the microwave signal to one of the two transmission paths.

The switches are controlled by the bias currents that can be injected into the circuit through the midpoint of a $\lambda/2$ open-circuited stub. The first $\lambda/4$ wider stub transforms the open-circuited load into a short circuit at the midpoint, and the next $\lambda/4$ narrower stub transforms it so that the main transmission line is not loaded. Two short-circuited high impedance $\lambda/4$ stubs provide a return path for the dc current return. When a dc current is applied to the top-right pad, it flows through the top signal line and there is no net current on the bottom line due to cancellation. Because the microbridges are much narrower than the rest of the conducting path, the current density at the bridges is much larger. As the current exceeds the superconducting critical current density at the bridges, they switch to a lossy or resistive state, forcing the microwave signal to propagate through the bottom line. The top signal line can be activated similarly when current is applied to the bottom-left pad. The bottom path is longer than the top by a length to create the desired shift in phase, which is 45° at 20 GHz in our design goal. Bias current needed to switch is about 20 mA.

Fig. 14 shows that our HTS phase shifter has a simulated insertion loss of less than 1 dB. This is a significant improvement over the conventional PIN diodes phase shifters that have an insertion loss of 3 dB per pair of switches plus additional conductor loss. The phase shift is 39° at 20 GHz. The simulation demonstrates that our HTS phase shifters potentially have accurate flat phase and amplitude response, low insertion loss, and low reflection, and low power dissipation. The HTS phase shifters are being fabricated and processed for performance testing.

IX. Conclusion

We have reviewed our recent activities in the design, simulation, fabrication, and testing of microwave coplanar transmission lines, resonators, switches and phase shifters using high temperature superconducting thin film technology. Our on-wafer probe and bit-error rate measurements show that the HTS transmission lines have extremely small insertion loss and dispersion. Two-dimensional HTS resonators with a very high unloaded Q have been designed for future use in cellular band stations. Power measurements on patterned HTS transmission line reveal a sharp switching feature that can be exploited for designs of analog switches as a replacement of conventional semiconductor PIN diode switches. These HTS switches can also be used in microwave phase shifters.

References

[1] G. B. Lubkin, "Applications of high-temperature superconductors approach the marketplace," *Phys. Today,* p. 20, Mar. 1995.

[2] A. Davidson, J. Talvacchio, M. G. Forrester, and J. R. Gavaler, "High-T_c materials expand superconductive circuit applications," *Microwaves & RF,* vol. 33, pp. 140–146, Apr. 1994.

[3] J. Kruse, R. A. Schweinfurth, F. Gao, D. Scherrer, D. Barlage, C. E. Platt, D. J. Van Harlingen, and M. Feng, "Cryogenic on-wafer microwave characterization of GaAs MESFET's and superconducting coplanar resonance and transmission lines structures," *Proc. SPIE High-T_c Microwave Superconductors Applicat.,* vol. V2156, p. 152, 1994.

[4] P. P. Nguyen, D. E. Oates, G. Dresselhaus, and M. S. Dresselhaus, "Nonlinear surface impedance for YBCO thin films: Measurements and a coupled-grain model," *Phys. Rev. B*, vol. 48, pp. 6400–6412, 1993.
[5] A. M. Ferendeci, S. L. Lu, C. M. Jackson, K. B. Bhasin, and C. Mueller, "High-T_c microwave superconductors and applications," in *Proc. SPIE*, R. B. Hammond and R. S. Whithers, Eds., 1994, vol. 2156, p. 116.
[6] C. Wilker, Z. Y. Shen, P. Pang, W. L, Holstein, and D. W. Face, "Nonlinear effect in high temperature superconductor: 3rd order intercept from harmonic generation," *IEEE Trans. Appl. Supercond.*, vol. 5, pp. 1665–1670, 1995.
[7] R. C. Taber, "A parallel plate resonator technique for microwave loss measurements on superconductors," *Rev. Sci. Instrum.*, vol. 61, pp. 2200–2206, 1990.
[8] F. Gao, M. V. Klein, J. Kruse, and M. Feng, "Mode coupling in superconducting parallel plate resonator with outer conductive enclosure,"*IEEE Trans. Microwave Theory Tech.*, to be published.
[9] F. Gao, J. W. Kruse, C. E. Platt, M. Feng, and M. V. Klein, "Microwave surface impedance at 10 GHz and quasiparticle scattering in $YBa_2Cu_3O_7$ films," *Appl. Phys. Lett.*, vol. 63, pp. 2274–2276, 1993.
[10] D. Kalokitis, A. Fathy, V. Rendricks, R. Brown, B. Brycki, E. Belahoubek, L. Nazar, B. Wilkens, T. Venkatesan, A. Tran, and X. D. Wu, "Removing packaging parasics effect," *J. Electronic Mater.*, vol. 19, p. 340, 1990.
[11] K. C. Gupta, R. Garg, and I. J. Bahl, *Microstrip Lines and Slotlines*. Norwood, MA: Artech House, 1979.
[12] J. W. Kruse, W. H. Chang, D. Scherrer, M. Feng, M. Scharen, A. Cardona, and R. Forse, "Eye-diagram and scattering parameter characterization of superconducting and gold transmission lines," *Appl. Phys. Lett.*, vol. 65, p. 2478, 1994.
[13] A. Porch, M. J. Lancaster, and R. G. Humphreys, "The coplanar resonator technique for determining the surface impedance of YBCO thin film," *IEEE Trans. Microwave Theory Tech.*, vol. 43, p. 306, 1995.
[14] F. Gao, Z. Zhou, M. Feng, M. Scharen, A. Cardona, and R. Forse, "Hysteresis effect in microwave power transmission of high temperature superconducting coplanar transmission lines," *Appl. Phys. Lett.*, vol. 67, pp. 2229–2231, 1995.
[15] J. Krupka, R. G. Geyer, M. Kuhn, and J. H. Hinken, "Dielectric properties of single crystals of Al_2O_3, $LaAlO_3$, $NdGaO_3$, $SrTiO_3$, and MgO at cryogenic temperatures," *IEEE Trans. Microwave Theory Tech.*, vol. 42, pp. 1886–1890, 1994.
[16] G. Liang, X. Dai, D. F. Hebert, T. van Duzer, N. Newman, and B. F. Cole, "High temperature superconductor resonators and phase shifters," *IEEE Trans. Appl. Supercond.*, vol. 1, pp. 58–66, 1991.

Milton Feng (M'82–SM'82–F'92), for a photograph and biography, see p. 952 of the June issue of this TRANSACTIONS.

Frank Gao (M'93), for a photograph and biography, see p. 952 of the June issue of this TRANSACTIONS.

Zhongmin Zhou, photograph and biography not available at the time of publication.

Jay Kruse (S'91–M'96), for a photograph and biography, see p. 952 of the June issue of this TRANSACTIONS.

Matt Heins, photograph and biography not available at the time of publication.

Jianshi Wang, photograph and biography not available at the time of publication.

S. Remillard, photograph and biography not available at the time of publication.

R. Lithgow, photograph and biography not available at the time of publication.

M. Scharen, photograph and biography not available at the time of publication.

A. Cardona, photograph and biography not available at the time of publication.

R. Forse, photograph and biography not available at the time of publication.